

DIRECT NUMERICAL SIMULATION OF A SQUARE JET EJECTED TRANSVERSELY INTO AN ACCELERATING, LAMINAR MAIN FLOW

Joshua R. Brinkerhoff

Department of Mechanical and Aerospace Engineering
Carleton University
1125 Colonel By Drive, Ottawa, Canada, K1S 5B6

Metin I. Yaras

Department of Mechanical and Aerospace Engineering
Carleton University
1125 Colonel By Drive, Ottawa, Canada, K1S 5B6
metin_yaras@carleton.ca

ABSTRACT

A direct numerical simulation of a square jet ejected transversely into a laminar boundary layer was performed at a jet-to-main-flow velocity ratio of 9.78 and a jet Reynolds number of 6330. The jet consisted of a single pulse with a duration equal to the time required for the jet fluid to travel 173 jet widths. A strongly-favorable streamwise pressure gradient was applied to the flat-plate flow and produced a freestream acceleration that is above the typical threshold required for relaminarization. The results of the simulation illustrate the effect of the favorable streamwise pressure gradient on the flowfield created by the transverse jet. The upwind shear layer of the jet is unstable to a Kelvin-Helmholtz-like instability and rolls-up into discrete shear-layer vortices. Vorticity from the jet shear layer accumulates near the corners of the jet and produces vertically-oriented vortex pairs near the upwind and downwind corners of the jet. The upwind pair couples with the shear-layer vortices to produce large, counter-rotating vortices in the freestream, while the downwind pair is unstable, and periodically produces hairpin-like vortices in the main-flow boundary layer and elongated, downwards-oriented vortices in the freestream behind the jet. The departure of the jet flowfield from that typically observed in transverse jets illustrates the effect of the favorable streamwise pressure-gradient on the flowfield created by the jet.

INTRODUCTION

The flowfield surrounding a jet ejected transversely into a flow has been the subject of extensive research. Transverse jets occur in numerous engineering applications, including in gas turbine engines when diluting high-temperature combustion products before they enter the turbine section (Vermeulen et al., 1992), in film cooling and active flow-control of turbine blades, in thrust-vectoring of rocket engines, and during the transition from vertical to forward flight in vertical take-off and landing aircraft (e.g. Karagozian, 2010). The transverse

jet achieves a high degree of near-field mixing largely due to the complex system of vortical structures that are created by the jet. Fric and Roshko (1994) categorized these structures into four groups, sketched in Figure 1: (i) shear-layer vortices; (ii) a counter-rotating vortex pair (CVP); (iii) a horseshoe vortex; and (iv) wake vortices. The shear-layer vortices are created by the periodic accumulation of circumferential vorticity in the direction of the jet due to a Kelvin-Helmholtz instability that is promoted by the inflectional velocity profile of the jet (e.g. Megerian et al., 2007). The subsequent interaction of these vortices with the main flow produces a counter-rotating vortex pair roughly aligned with the jet trajectory (e.g. Yuan et al., 1999; Lim et al., 2001; Cortelezzi and Karagozian, 2001). The horseshoe vortex is created near the wall upstream of the jet by the separation and subsequent roll-up of the main-flow boundary layer in response to an adverse pressure-gradient induced upstream of the jet (Kelso and Smits, 1995). Vertically-aligned, counter-rotating wake vortices in the rear of the jet span from the jet trajectory to the wall in a manner similar to the vortex sheet behind a solid cylinder. However, unlike a cylinder, freestream streamlines close around the rear of the jet (Morton and Ibbetson, 1996), producing a local adverse pressure-gradient region behind the jet that causes separation of the main-flow boundary layer, and the subsequent reorientation and entrainment of the separated boundary-layer vorticity results in the wake vortices.

The flowfield produced by a transverse jet is evidently strongly connected to the development of the main-flow boundary layer and the jet shear-layer. Little attention has been given, however, to the effect of the main-flow freestream conditions, particularly the streamwise pressure gradients applied to the main flow. To address this question, a direct numerical simulation (DNS) was performed of a jet that is ejected transversely into an accelerated, laminar boundary layer. A strongly-favorable streamwise pressure gradient was imposed on the flat plate with the expectation that the resulting freestream acceleration would stabilize the flat-plate boundary

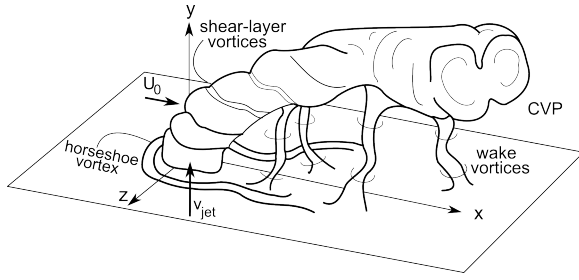


Figure 1. Schematic of vortical structures in the flowfield of a transverse jet. Adapted from Karagozian (2010).

layer so that the structures resulting from the interaction of the jet and main flows would be more organized and thus easier to detect and study. The results provide insight on the transient formation of the vortical flow structures that are created in this scenario and how they are affected by a strongly-favorable streamwise pressure gradient applied to the main flow.

NUMERICAL METHOD

The computational domain, shown in Figure 2, consists of a main-flow sub-domain containing a flat, no-slip test surface and a jet sub-domain comprised of a rectangular pipe. The jet sub-domain has dimensions of $D = 2.2$ mm and a wall-normal length of $10D$, and the main-flow sub-domain has streamwise and spanwise dimensions of $250D$ and $50D$, respectively. The wall-normal height of the main-flow sub-domain at the leading edge is $114.5D$. A uniform, time-invariant velocity of 4 m/s parallel to the test surface and a static pressure that remains fixed in an area-averaged sense are specified at the inflow and outflow boundaries of the main-flow sub-domain, respectively, and the sides and upper wall are specified as free-slip walls. The level of freestream acceleration is adjusted by sloping the upper wall towards the test surface by 5.6° . The centerline of the jet orifice is located at the midspan of the test surface and $80D$ from the test-surface leading edge. The sides of the jet sub-domain are specified as no-slip walls to allow development of the boundary layer within the jet. A spatially-uniform velocity of 35 m/s is applied at the inlet of the jet sub-domain for a duration of $t_{jet} = 8.65$ ms. Growth of the jet boundary layer along the walls of the jet sub-domain accelerates the core flow in the jet to a value of $v_{jet} = 44$ m/s at the center of the jet orifice, and the resulting jet velocity ratio is $r = v_{jet}/U_0 = 9.78$; the reference velocity $U_0 = 4.5$ m/s is defined as the freestream velocity at a wall-normal height of $16D$ above the center of the jet orifice when the jet is turned off.

A structured grid consisting of hexahedral finite volumes was mapped to the test-surface and jet sub-domains described above. The main-flow sub-domain is discretized with 345, 88, and 197 nodes in the streamwise, wall-normal, and spanwise directions, respectively. In the jet sub-domain, the directions normal to the jet flow (x and z) are discretized with 60 nodes, spaced to place at least 20 nodes in the jet boundary layer, while the direction parallel to the jet flow is discretized with 88 nodes that are distributed to provide the highest spatial resolution near the jet orifice.

ANSYS CFX [®] (Version 12), a commercial

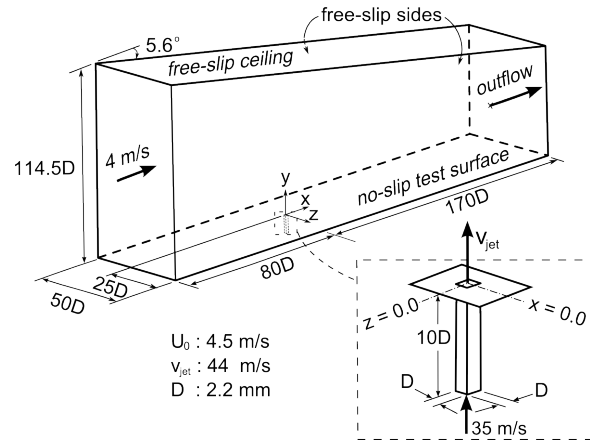


Figure 2. Schematic of the computational domain. A magnified view of the jet sub-domain is shown in the dashed box.

computational-fluid-dynamics software package, was used to solve the incompressible form of the time-varying mass- and momentum-conservation equations through a finite-volume approach. Discretization of the governing equations is based on central differencing and second-order Euler backward differencing for the spatial and temporal derivatives, respectively. To resolve the transient interaction between the jet and the main-flow boundary layer, a temporal resolution is chosen such that the jet flow takes about 10 timesteps to penetrate a distance equivalent to the displacement thickness of the main-flow boundary layer at the jet orifice, resulting in a timestep size of $\Delta t = 7 \times 10^{-6}$ s. The discretized equations are converged through an algebraic multigrid scheme within eight inner-loop iterations per timestep, reducing the root-mean-square residual of the governing equations by five orders of magnitude to less than 10^{-6} . Approximately 20,000 timesteps are required for the laminar main-flow boundary layer to reach a steady state, after which the vertical jet is impulsively turned on for 8.65 ms—which corresponds to 1236 timesteps—and then impulsively turned off, and the simulation is then continued for 6400 more timesteps.

RESULTS AND DISCUSSION

The distribution of the freestream velocity and acceleration parameter in the main flow in the absence of the jet is shown in Figure 3. The acceleration parameter, defined as $\eta = \nu/U_e^2 dU_e/dx$, where U_e is the local boundary-layer edge velocity, is observed to exceed the critical acceleration parameter range, beyond which a turbulent boundary layer will begin to relaminarize (Escudier et al., 1998). It was expected that by stabilizing the main-flow boundary layer to this extent, structures created through the interaction of the main-flow with the jet would be more organized and their transient development would occur more slowly and thus could be studied more precisely. Figure 3 also plots the steady boundary-layer displacement thickness that was present along the length of the test surface prior to activation of the jet. Downstream of the jet, the displacement thickness remains approximately constant, as the growth of the main-flow boundary layer is

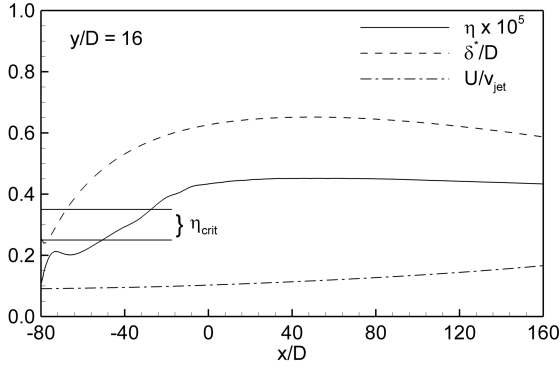


Figure 3. Streamwise distribution of acceleration parameter (η), displacement thickness (δ^*/D), and freestream velocity (U/v_{jet}) in the main flow.

hindered by the strong freestream acceleration.

The jet velocity ratio in the present study is sufficiently large that the jet flow ejected from the orifice has enough momentum to penetrate through the main-flow boundary layer and into the freestream. Figure 4 illustrates the effect that the jet has on the time-averaged main flow by plotting time-averaged streamlines and pressure coefficient contours (defined as $\overline{C_p} = \overline{p}/0.5\rho v_{jet}^2$) at several wall-normal planes within the main-flow boundary layer and freestream. At a wall-normal height of $y/D = 1.800$, which is well into the freestream, streamlines deflect around the sides of the jet and then close tightly behind the rear of the jet, producing a non-uniform pressure field as shown by the $\overline{C_p}$ contours. As this non-uniform pressure field is projected onto the test surface, it promotes the separation of the main-flow boundary layer. This is clearly seen in the $y/D = 0.023$ plane; the points at which the streamlines converge are the locations where the separated boundary layer detaches from the wall and is entrained vertically into the transverse-jet flow. The $y/D = 0.167$ plane shows that further from the wall, the separated fluid joins vertically-oriented vortices that originate near the upwind and downwind corners of the jet orifice, termed ‘‘corner vortices’’. Further away from the wall, the $y/D = 0.905$ plane shows that the upwind corner vortices begin to bend downwind due to the increased momentum of the main flow. By the $y/D = 1.800$ plane, the downwind vortex pair appears to have merged with the upwind pair. It is shown below, however, that the corner vortices have not actually merged but the downwind pair undergoes a transient development that results in its apparent disappearance from the time-averaged flowfield.

The development of vortical structures created through the interaction of the jet and main flow during the initial transient development of the jet is shown in Figure 5 through iso-contours of the second-invariant of the velocity-gradient tensor normalized by v_{jet}/D , denoted Q . The iso-contours are shaded according to the wall-normal height to aid in distinguishing the relative heights of the various flow structures. For brevity in this section, the acronyms defined in Figure 5 will be used to refer to the vortices. At $\tau = 1$ a square vortex loop (denoted VL) is ejected from the orifice and is convected upwards at a speed of about half the jet velocity due to its origin in the slower-moving fluid in the jet boundary-layer.

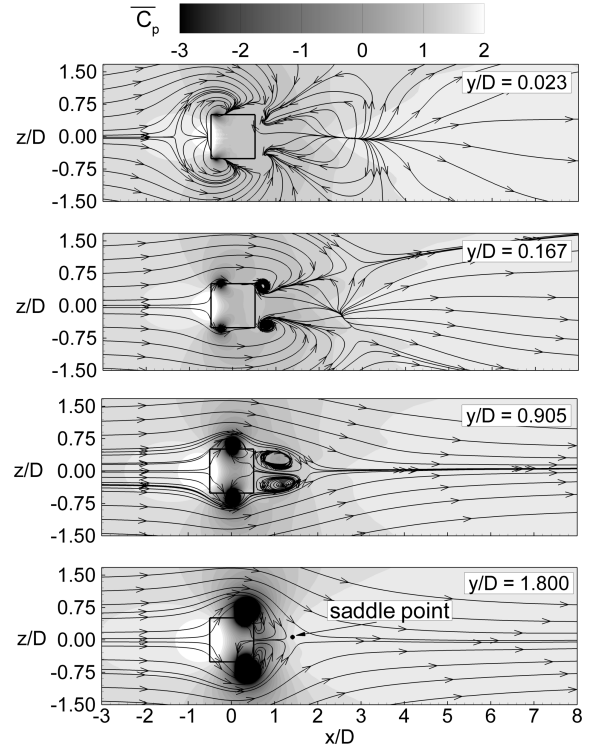


Figure 4. Wall-normal development of the jet flowfield, shown through time-averaged streamlines and pressure coefficient contours. The projection of the jet orifice is shown by the black square.

The corners of the VL are turned upwards slightly due to the velocities induced by the vorticity contained in the loop. By $\tau = 4$, narrow upright vortices are created at the corners of the jet. These correspond to the upwind and downwind corner vortices (denoted UCV and DCV, respectively) observed in Figure 4. The UCV and DCV are created through the accumulation of jet vorticity in the corners of the jet due to the velocities induced on the jet by the VL and the non-uniform pressure field surrounding the jet, as seen in Figure 4. The velocity induced by the VL pushes the corner vortices into the higher-momentum flow at the center of the jet so that by $\tau = 6$, the UCV and DCV have been convected above the VL. Simultaneously, the UCV and DCV induce velocities on each other that brings the DCV pair closer while driving the UCV pair further apart. Since the vortex lines associated with these vortices cannot end in the vorticity-free fluid, by $\tau = 9$ the top of the DCV pair are seen to connect to each other (as they are in close proximity) while the UCV pair (which are further apart) couple with the vorticity in the VL.

Discrete, approximately spanwise-oriented shear-layer vortices (denoted SLV) become evident at $\tau = 9$. These vortices are created through a Kelvin-Helmholtz-like instability of the jet shear layer, leading to periodic roll-up of the shear layer into the discrete SLVs at a frequency (expressed as a Strouhal number $St = fD/v_{jet}$) of $St = 0.52 - 0.57$. At the same time, the VL begins to tilt downwind due to the enhanced entrainment of slower-moving main-flow fluid on the downwind side of the VL. At $\tau = 12$, the velocity induced by

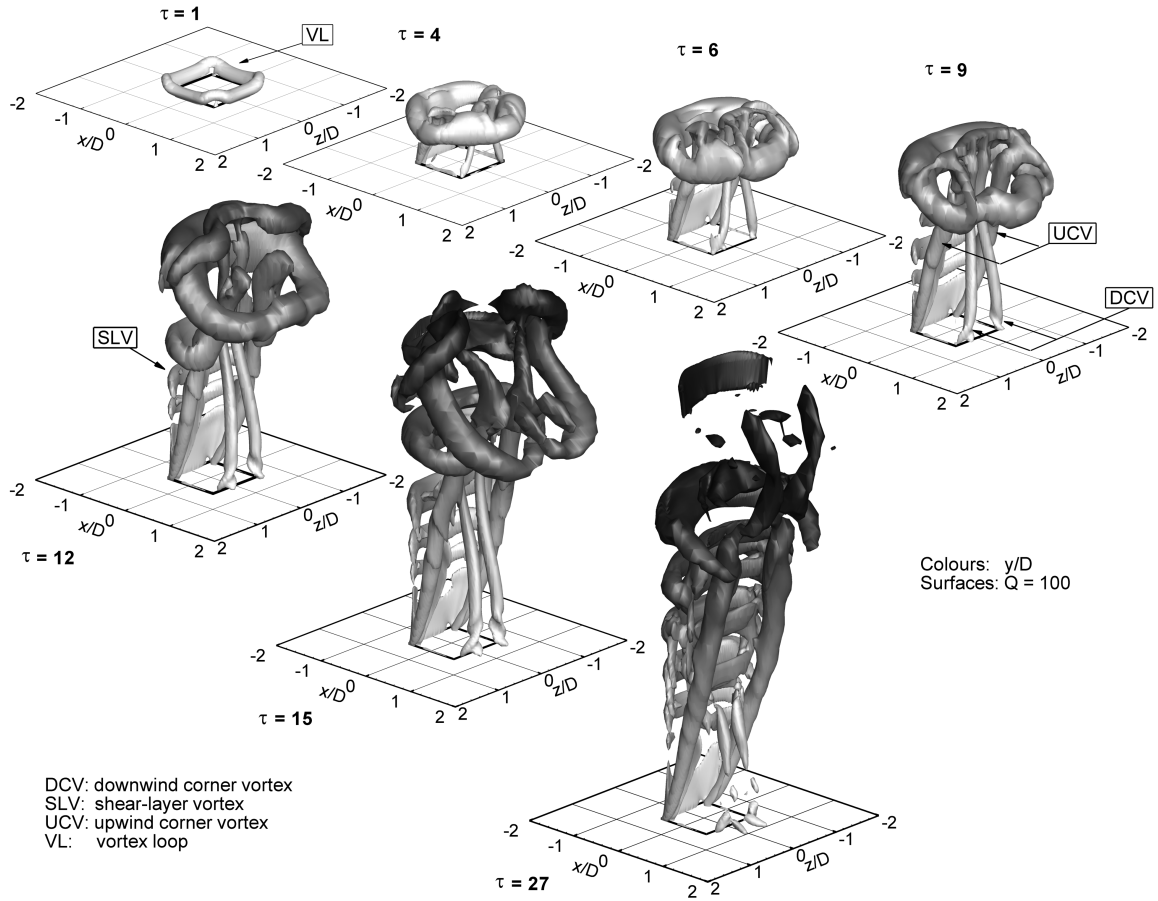


Figure 5. Vortical structures observed in the transverse jet during its initial transient development. Iso-contours are of Q and are shaded according to y/D .

the VL pulls the legs of the first-shed SLV upward through the middle of the VL. Subsequently-shed SLVs are further away from the VL and are not influenced to the same extent, so their legs point downwards and connect to the upwind jet shear-layer. The downwards-pointing shape is consistent with the folding of the shear-layer vortices described by Kelso et al. (1996) and others. At $\tau = 15$, the top of the UCV, the legs of the first SLV, and the downwind-tilted VL interact in a way that breaks-down the VL so that at $\tau = 27$ it is no longer visible. Simultaneously, the UCV is convected in the wall-normal direction by the jet fluid and its cross-section increases as the induced velocity field entrains main-flow fluid that is brought into the rear of the jet by the adverse streamwise pressure gradient set up behind the jet, as seen in Figure 4. As the UCV stretches into the freestream, it is tilted downwind by the main flow while still entraining main-flow fluid, becoming the streamwise-oriented counter-rotating vortex pair (CVP) that is a common feature of transverse jets and is responsible for the majority of the mixing of the jet fluid with the main flow (Haven and Kurosaka, 1997).

The continued development of the vortical structures in the jet flowfield is shown in Figure 6, which plots iso-contours of Q at a lower value in order to visualize the weaker structures downwind of the jet. The spatial location of the UCV remains quite steady throughout the jet lifetime, while the DCV

appears to be highly unsteady. At $\tau = 30$, a hairpin-like vortex loop is created near the wall downwind of the jet. This structure is created as follows: the velocity field induced by the DCV (labeled 1) causes the spanwise-oriented vorticity that is constantly being ejected from the downwind side of the orifice to be re-oriented in the streamwise direction. The reoriented vorticity then induces a velocity on the DCV that draws the bottoms of its right and left legs nearer to the orifice and to each other. Eventually, the legs of the DCV are brought close enough that they merge and form a hairpin-like vortex loop with legs pointing in the downwind direction. The bending of the legs of the DCV is visible at $\tau = 30$, the coupling of the legs of the DCV can be seen at $\tau = 60$, and the growth and movement of the resulting vortex loop is seen at $\tau = 90$. The vortex loop remains embedded in the main-flow boundary layer and grows laterally and longitudinally as it convects downwind. At $\tau = 90$, a second DCV (labeled 2) is seen forming from the vorticity that is being ejected from the jet and from the vorticity of the main-flow boundary layer behind the jet as it separates from the wall under the influence of the adverse pressure gradient. As the second-generation DCV grows, it undergoes the same process to produce a second hairpin-like vortex loop, which is visible in the near-wall region slightly upwind of the previously-created structure at $\tau = 120$. The creation of the DCV and its subsequent evolu-

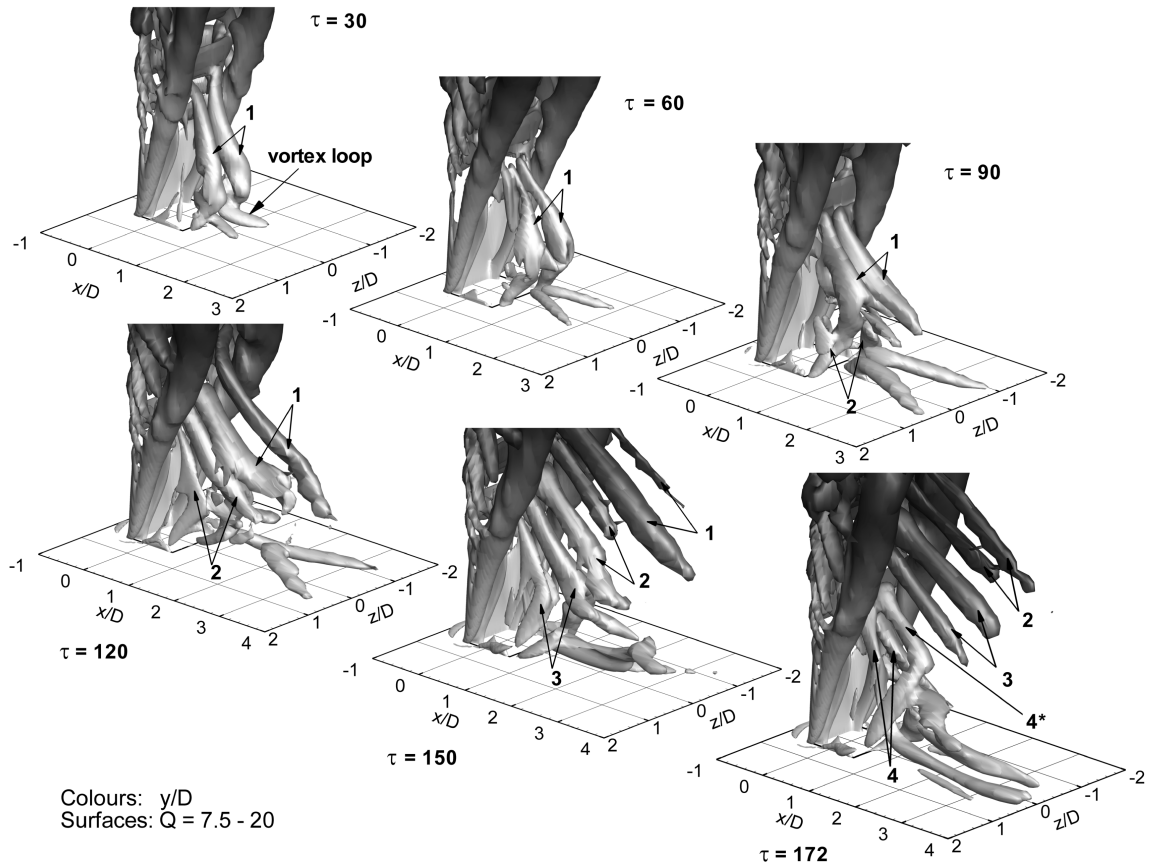


Figure 6. Vortical structures observed in the transverse jet. Iso-contours are of Q and are shaded according to y/D .

tion to form a hairpin-like structure repeats periodically until the fourth generation, after which the jet duration has completed and the jet flow turns off.

Figure 6 at $\tau = 60$ shows that after the hairpin-like structure is created from the near-wall portion of the DCV, the two segments of the DCV that are located further away from the wall connect to each other. As it does so, the DCV entrains main-flow fluid that is moving upwards in the rear of the jet. Since the top of the DCV is still connected to the downwind side of the jet shear layer, entrainment of vertically-moving fluid causes the now-connected legs of the DCV to rotate upwards, producing elongated structures angled at about 45° to the vertical. This angle decreases (i.e. the structures become more horizontal) as the structures entrain more of the main-flow fluid while convecting away from the wall. As each generation of DCV breaks down to produce a hairpin-like vortex loop in the main-flow boundary layer, the process yielding the elongated, downwards-pointing vortices also repeats. The labels in Figure 6 distinguish the third- and fourth-generation structures as they are created and convected upwards in the rear of the jet.

At $\tau = 172$, a DCV pair (labeled 4) is seen to begin to break down into a hairpin-like structure. Just above that, the structure labeled 4* is a DCV that did not break-up into a hairpin-like structure but remained as a single vortex with a roughly-vertical alignment. The further evolution of this structure in time cannot be studied because the jet flow was

turned off shortly after $\tau = 172$, but the structure appears similar to the upright wake vortices that are commonly observed in the wakes of transverse jets but are absent in the current study. Fric and Roshko (1994) attribute wake vortices to the entrainment and reorientation of boundary-layer vorticity after the main-flow separates from the wall downwind of the jet due to the local adverse pressure-gradient, which is similar to the explanation given above for the creation of the hairpin-like structures and downwards-pointing vortices observed in the current study. This suggests that the mechanism for the creation of wake vortices is present in the current study but the conditions are not suitable for full-sized wake vortices to be created. Again, Fric and Roshko (1994) observed that the shedding of wake vortices is most distinct at a velocity ratio of $r = 4$; below this ratio, the jet is too close to the main-flow boundary layer and the wake vortices get mixed with other structures, while above this ratio the jet is more upright and entrainment of the separated main-flow vorticity is more difficult. These observations suggest that the absence of wake vortices in the current study may be partially due to the relatively high velocity ratio ($r = 9.78$), but the favorable stream-wise pressure-gradient applied to the main flow is probably the dominant factor. Freestream acceleration not only stabilizes the vortical structures ejected from the jet but it also delays the separation of the main-flow boundary layer at the rear of the jet. By weakening separation, the flow conditions may no longer favor the creation of full-size wake vortices,

and instead produce the observed hairpin-like vortex loops in the main-flow boundary layer and the elongated, downwards-pointing vortices in the freestream.

Once the jet stops ejecting vorticity, the vortical structures in the freestream are swept downwind and interact with each other and the main flow such that they dissipate quite rapidly. The hairpin-like vortex loops created in the main-flow boundary layer are stabilized by the favorable streamwise pressure gradient and thus remain embedded in the main-flow boundary layer and convect downstream at a fraction of the boundary-layer edge velocity. The mutual interaction and break-down of these structures into a region of locally-turbulent flow—which appears quantitatively similar to a turbulent spot—is the subject of a subsequent study.

CONCLUSIONS

Direct numerical simulation was used to study the flowfield created by a square jet ejected transversely through a laminar, accelerating main flow. A jet with a velocity ratio of $r = 9.78$ was impulsively ejected for a duration equivalent to the time required for the jet fluid to travel 173 jet widths. A strongly-favorable streamwise pressure gradient was applied to the main flow to understand the effect of freestream acceleration on the coherent flow structures created in the jet flowfield. Vorticity at the upwind and downwind corners of the jet forms two pairs of vortices. The pair originating in the upwind corners are fed primarily by main-flow fluid entrained from the sides and rear of the jet. This pair remains relatively steady and eventually forms the counter-rotating vortex pair in the freestream above the test surface. The vortex pair originating in the downwind corners of the jet is fed primarily by vorticity that is reoriented and entrained from the main-flow boundary layer as it separates downwind of the jet in response to the local adverse pressure gradient. This pair is highly unsteady and its induced velocity field leads to an instability that produces hairpin-like vortex loops in the main-flow boundary layer downwind of the jet and highly-elongated, downwards-oriented vortices in the freestream. The development of these flow structures, rather than the upright vortices typically observed in the wakes of transverse jets, is attributed to the stabilization of the main-flow boundary layer by the favorable streamwise pressure gradient, and the reduction in the local adverse pressure gradient prevailing in the wake of the jet, thus altering the local separation of the main-flow boundary layer from the test surface.

REFERENCES

- Cortelezzi, L. and Karagozian, A. R. (2001), “On the Formation of the Counter-Rotating Vortex Pair in Transverse Jets”, *Journal of Fluid Mechanics*, Vol. 446, pp. 347–373.
- Escudier, M. P., Abdel-Hameed, A., Johnson, M. W. and Sutcliffe, C. J. (1998), “Laminarization and Retransition of a Turbulent Boundary Layer Subjected to a Favourable Pressure Gradient”, *Experiments in Fluids*, Vol. 25, pp. 491–502.
- Fric, T. F. and Roshko, A. (1994), “Vortical Structure in the Wake of a Transverse Jet”, *Journal of Fluid Mechanics*, Vol. 279, pp. 1–47.
- Haven, B. A. and Kurosaka, M. (1997), “Kidney and Anti-Kidney Vortices in Crossflow Jets”, *Journal of Fluid Mechanics*, Vol. 352, pp. 27–64.
- Karagozian, A. R. (2010), “Transverse Jets and Their Control”, *Progress in Energy and Combustion Science*, Vol. 36, pp. 531–553.
- Kelso, R. M., Lim, T. T. and Perry, A. E. (1996), “An Experimental Study of Round Jets in Cross-Flow”, *Journal of Fluid Mechanics*, Vol. 306, pp. 111–144.
- Kelso, R. M. and Smits, A. J. (1995), “Horseshoe Vortex Systems Resulting From the Interaction Between a Laminar Boundary Layer and a Transverse Jet”, *Physics of Fluids*, Vol. 7, pp. 153–158.
- Lim, T. T., New, T. H. and Luo, S. C. (2001), “On the Development of Large-Scale Structures of a Jet Normal to a Cross Flow”, *Physics of Fluids*, Vol. 13, pp. 770–775.
- Margason, R. J. (1993), Fifty Years of Jet in Crossflow Research, in ‘Computational and Experimental Assessment of Jets in Cross Flow’, number CP-539, AGARD Rept CP-539.
- Megerian, S., Davitian, J., de B. Alves, L. S. and Karagozian, A. R. (2007), “Transverse-Jet Shear-Layer Instabilities. Part 1. Experimental Studies”, *Journal of Fluid Mechanics*, Vol. 593, pp. 93–129.
- Morton, B. R. and Ibbetson, A. (1996), “Jets Deflected in a Crossflow”, *Experimental Thermal and Fluid Science*, Vol. 12, pp. 112–133.
- Vermeulen, P. J., Grabinski, P. and Ramesh, V. (1992), “Mixing of an Acoustically Excited Air Jet With a Confined Hot Crossflow”, *Journal of Engineering for Gas Turbines and Power*, Vol. 114, pp. 46–54.
- Yuan, L. L., Street, R. L. and Ferziger, J. H. (1999), “Large-eddy Simulations of a Round Jet in Crossflow”, *Journal of Fluid Mechanics*, Vol. 379, pp. 71–104.